การประเมินอัลกอริธึมสำหรับการสร้างรูปร่างของคุณสมบัติเปลวเพลิงโดยวิธีโทโมกราฟฟี

Evaluation of An Algorithm for Tomographic Reconstruction of Flame-property Profiles

P. Meekunnasombat

P. Vallikul

B. Fungtammasan

Department of Mechanical Engineering

King Mongkut's Institute of Technology

North Bangkok

Bangsue Bangkok 10800

บทความฉบับนี้ได้ศึกษาถึง ความถูกต้องในการสร้างภาพเสมือนของคุณสมบัติต่าง ๆ ของเปลวไฟที่มีรูปร่างสมมาตรและไม่สมมาตรกับแกน ด้วยวิธีฟิลเตอร์แบ็คโปรเจ็คชั่น โดยรูปร่างของเปลวที่ใช้ศึกษาได้จำลองขึ้นด้วยคอมพิวเตอร์ การศึกษาครั้งนี้พยายามหาผลกระทบของรูปร่างเปลว , ความถี่ในการเก็บตัวอย่างตามแนวขวางและแนวเส้นรอบวง และสัญญาณรบกวนในการเก็บตัวอย่าง ที่มีผลต่อภาพเสมือนที่สร้างขึ้น โดยได้ทำการประเมินความแตกต่างในเชิงปริมาณระหว่างรูปร่างของเปลวตัวอย่างในการทดสอบกับภาพเสมือนที่สร้างขึ้น จากการศึกษาพบว่า วิธีฟิลเตอร์แบ็คโปรเจ็คชั่นนี้สามารถขจัดสัญญาณรบกวนได้ดี เนื่องจากองค์ประกอบที่เป็นความถี่สูงมักถูกกำจัดไปด้วยผลของการกรอง และวิธีนี้สามารถนำไปใช้ได้กับการสร้างภาพเสมือนของรูปร่าง 2 มิติใด ๆ

The Filter Back-projection method is used to reconstruct axisymmetrical and asymmetrical flame-property profiles from their computer simulated projection functions. The effect of the mathematical shape of the profiles, the lateral and angular sampling rates and of the measurement noise on reconstruction accuracy are studied. Deviations between the test profile and the reconstructed profile are quantitatively evaluated. Their dependence on the filter functions and on the sampling rates are also examined. It has been found that reconstruction by the Filter Back-projection method is very tolerant of noise, since high frequency terms tend to be removed by filtering and that the method is capable of reconstructing an arbitrary 2-D function.

1. Introduction

Absorption Tomography is an optical measurement technique for monitoring thermodynamic properties in combustion flames. By this method, two-dimensional property fields across a flame are reconstructed from their multi-angular path measurement projection data (see Fig.1). This provides a major advantage over customary optical point measurement techniques in that the property fields of species with low concentration for all points in the flame cross-sections can be reconstructed simultaneously from the same set of projection data.

For absorption measurement in a homogeneous media, a monochromatic pencil beam of ray having an intensity I_0 , when passing through a uniform medium, is attenuated in accordance with Beer's law,

$$I = I_0 e^{-Ks}$$

where K is the absorption coefficient and I is the emerging intensity after attenuation along the path length s.

In gaseous mixtures, the absorption coefficient K, in the thermal model is both temperature dependent and nonhomogeneous. Hughey and Santavicca [1] rewrite Beer's law in the form

$$I = I_0 e^{(-\int pP_\omega ds)}$$

where $K = pP_\omega$, p is the partial pressure of the absorbing species, P_ω ($cm^{-1}atm^{-1}$) the volume absorption coefficient at frequency ω , and s the optical path length. The projection functions can be found experimentally from the absorption data, hence,

$$p_\theta(r) = \int_{source}^{detector} pP_\omega ds = -ln\frac{I}{I_0} .$$

Tomographic techniques provide solutions to this equation for pP_ω which is in turn a function of gas temperature and concentration. The "two-line" method is used to obtain the temperature and absorbing species concentration [1]. This method involves making two sets of line center absorption measurements at different wavelengths. The knowledge of the line center absorption coefficients and their temperature dependence is readily available from the literature [2]. Hughey and Santavicca [1] assumed as a simplification, that the absorption coefficients vary linearly with temperature. A linear absorption model for the R(6) and R(19) lines of the CO 4.7μ band [1] was extrapolated to high temperature to give the empirical relations:

$$P_{\omega_1} = 58.1 - 0.024T$$

$$P_{\omega_2} = -18.99 + 0.092T.$$

These are used in the reconstruction process. Substituting these equations into the reconstruction results in

$$f_i(x,y) = pP_{\omega_i}(x,y) \ , \quad i = 1,2$$

and solving for the temperature gives

$$T(x,y) = \frac{58.1 f_2(x,y) + 18.99 f_1(x,y)}{0.092 f_1(x,y) + 0.024 f_2(x,y)} \ .$$

Once the temperature is known , $p(x,y)$ can then be calculated and the concentrations are found through the equation of state. The key to the combustion tomography problem is to accurately reconstruct the 2-D absorption coefficient functions from their 1-D projections.

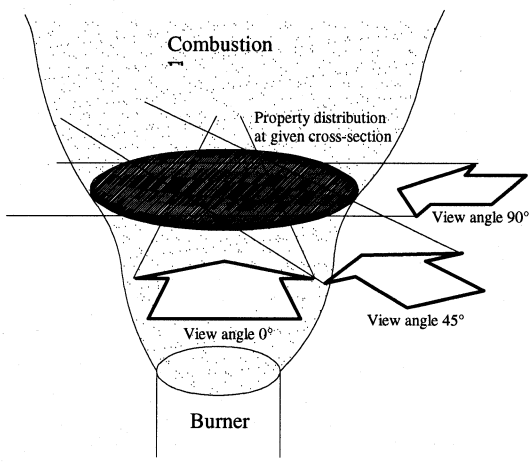

Figure 1 A typical scanning from tomographic measurement

Chen and Goulard [2] introduced a generalized onion peeling inversion method to measure pollutant emitted from jet engine exhaust flows. The method determines the two-dimensional property fields, beginning at the exterior shell, proceeding inward shell by shell as in a peeling process. The technique is very sensitive to measurement noise such that errors accumulate with the peeling process, leading to unstable solutions. Emmerman, et al [3] overcame the accumulation errors by introducing a mathematical transform technique called Filter Back-projection (FBP) technique. The FBP technique transforms the absorption data into the frequency domain where noisy components can be truncated. Hughey and Santavicca [1] pointed out in their computer simulated noisy absorption measurement data of axisymmetric reacting flow fields that the FBP outperforms the onion peeling. The FBP also has advantage over customary Abel transform [4] techniques in that it can reconstruct a more general 2-D function. Although the FBP technique is very tolerant of noise, frequency response of different filter functions and the averaging nature of the 2-D mathematical transform have to be studied.

In this paper, mathematical profiles are reconstructed from their computer simulated projection data, using the classical FBP algorithm. Reconstruction from synthetic projections allows the reconstruction algorithm to be evaluated independently of measurement noise. Effects of lateral and angular sampling frequencies, of obstacles along the absorption paths and of fictitious noise on the reconstruction results are studied.

2. Definitions

The test functions, their projections and the "Picture distance" which is used to evaluate the resemblance between the reconstruction results and the test functions are mathematically defined in this section.

2.1 The Test Functions

Three test functions are employed in this paper. These are: Gaussian, multi-layer top hat, and a combination of an off-center Gaussian profiles and three ellipsoidal. The Gaussian profile (Fig.3) is defined by

$$f(x,y) = e^{-c(x^2+y^2)} \ ,$$

where the constant "c" is set to be 20.

A multi-layer top hat profile (Fig.4) is the summation of co-center top hat profiles of different radii, hence,

$$f(x,y) = \begin{cases} \rho_i & for \quad x^2 + y^2 \le A_i^2 \\ 0 & otherwise \ , \end{cases}$$

ρ_i are set to be 0.2, 0.5, 0.7 and 1.0 when A_i equal 0.65, 0.50, 0.35 and 0.20 correspondingly.

The third test function is a combination of an off-center Gaussian profile, an ellipse, a hollow cylinder, confined in a circular wall (Fig.12c). We write

$$f(x,y) = f_1 + f_2 + f_3 + f_4$$

$$f_1 = e^{-c[(x-x_1)^2 + (y-y_1)^2]} \ .$$

The constant c , x_1 and y_1 are 20, 0.24 and 0.24 respectively.

$$f_2 = \begin{cases} \rho & for \ \frac{p^2}{A^2} + \frac{q^2}{B^2} \le 1 \\ 0 & otherwise \ , \end{cases}$$

where ρ , A and B are 0.3, 0.35 and 0.15 respectively while functions p and q are defined by

$$p = (x - x_1)\cos\theta + (y - y_1)\sin\theta$$
$$q = (y - y_1)\cos\theta - (x - x_1)\sin\theta \ ,$$

where x_1 , y_1 and θ are 0.2 , -0.4 and 20 degree respectively.

$$f_3 = \begin{cases} \rho & for \ r_{in} \le (x - x_1)^2 + (y - y_1)^2 \le r_{out} \\ 0 & otherwise \ , \end{cases}$$

where ρ , r_{in} , r_{out} , x_1 and y_1 are 0.2, 0.1, 0.24, -0.4 and 0.1 respectively.

$$f_4 = \begin{cases} \rho & for \ r_{in} \le x^2 + y^2 \le r_{out} \\ 0 & otherwise \ , \end{cases}$$

where ρ , r_{in} and r_{out} is 0.2, 0.8 and 0.9 respectively.

2.2 The Projections

A projection is a mapping of a two-dimensional function into a one-dimensional one, which can be obtained by integrating the function in a particular direction. The projection of $f(x,y)$ along $\theta^{\perp}$- direction is

$$p_\theta(r) = \int_{-\infty}^{\infty}\int_{-\infty}^{\infty} f(x,y)\delta(x\cos\theta + y\sin\theta - r)dxdy \ ,$$

where $\delta(x)$ is defined by,

$$\delta(x) = \begin{cases} 1 & x = 0 \\ 0 & \text{otherwise.} \end{cases}$$

We may interpret f in the (r,s) coordinate system, rotating from (x,y) coordinate system by the angle θ . With this representation, the integral is along the s-axis and the projection function can be written as

$$p_\theta(r) = \int_{-\infty}^{\infty} f_\theta(r,s)ds \ .$$

The projection function of Gaussian profile is

$$p(r) = \sqrt{\frac{\pi}{c}}e^{-cr^2} \ .$$

The projection function of the multi-layer top hat profile is

$$p(r) = \begin{cases} 2\rho_i\sqrt{A_i^2 - r^2} & \text{for } |r| < A_i \\ 0 & \text{otherwise} \ , \end{cases}$$

where ρ_i equals 0.2, 0.5, 0.7 and 1.0 when A_i being set at 0.65, 0.50, 0.35 and 0.20 respectively. Subscript θ has been omitted since both the Gaussian and the multi-layer top hat functions are axisymmetric.

The projection function of the combination of off-center Gaussian profile and the three ellipsoidal functions is

$$p_\theta(r) = p_\theta^1(r) + p_\theta^2(r) + p_\theta^3(r) + p_\theta^4(r) \ ,$$

$$p_\theta^1(r) = \sqrt{\frac{\pi}{c}}e^{-c(r-R)^2} \ ,$$

where $R = \sqrt{x_1^2 + y_1^2}\cos\{[\tan^{-1}\left(\frac{y_1}{x_1}\right)] - \theta\}$.

Functions $p_\theta^2(r)$, $p_\theta^3(r)$ and $p_\theta^4(r)$ are built from

$$p_\theta(r) = \begin{cases} \frac{2\rho AB}{a^2(\theta-\alpha)}\sqrt{a^2(\theta-\alpha) - (r-R)^2} & \\ & for \ |r| \le a(\theta - \alpha) \\ 0 & for \ |r| > a(\theta - \alpha), \end{cases}$$

where,

$$a^2(\theta-\alpha) = A^2\cos^2(\theta-\alpha) + B^2\sin^2(\theta-\alpha)$$

$$and \quad R = \sqrt{x_1^2 + y_1^2}\cos\{[\tan^{-1}\left(\frac{y_1}{x_1}\right)] - \theta\} \ .$$

The constants x_1, y_1, A, B, α and ρ corresponding to each projection function are shown in Table1. Descriptive meaning of these constants are shown in Fig.2.

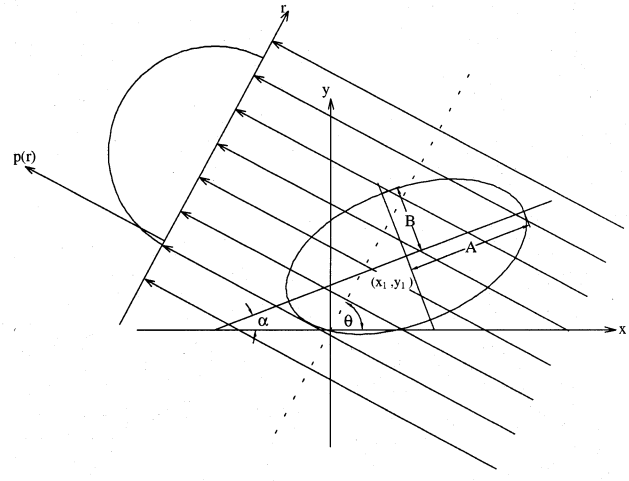

Figure 2 Descriptive meaning of the parameters of an ellipse.

Table 1 Constants in the projection with obstacles

Obstacle	x_1	y_1	A	B	α	ρ
$p_\theta^2(r)$	0.2	-0.4	0.35	0.15	20°	0.3
$p_\theta^{3,1}(r)$	-0.4	0.1	0.24	0.24	0°	0.2
$p_\theta^{3,2}(r)$	-0.4	0.1	0.1	0.1	0°	0.2
$p_\theta^{4,1}(r)$	0.0	0.0	0.9	0.9	0°	0.2
$p_\theta^{4,2}(r)$	0.0	0.0	0.8	0.8	0°	0.2
$p_\theta^3(r) = p_\theta^{3,1}(r) - p_\theta^{3,2}(r)$			$p_\theta^4(r) = p_\theta^{4,1}(r) - p_\theta^{4,2}(r)$			

2.3 Picture Distance

In order to evaluate the resemblance between the test profile and its reconstruction result, we used the concept of "Picture distance" [5]: it is the normalized root-mean-square distance, d, as defined by

$$d = \sqrt{\frac{\sum_{j=n}^{N}\sum_{k=m}^{M}(T_{j,k} - R_{j,k})^2}{\sum_{j=n}^{N}\sum_{k=m}^{M}(T_{j,k} - T_{mean})^2}} ,$$

where $T_{j,k}$ is the value of original profile, $R_{j,k}$ is the reconstruction, and T_{mean} the average value of $T_{j,k}$ over the region of interest.

3. Filter Back-Projection (FBP) algorithm [6]

3.1 Projection-Slice Theorem

Consider two-dimensional Fourier transform of $f(x,y)$,

$$F(X,Y) = \int_{-\infty}^{\infty}\int_{-\infty}^{\infty} f(x,y)e^{-i(Xx+Yy)}dxdy .$$

Rotate the function $f(x,y)$ to a new (r,s) coordinate system.

$$F(X,Y) = \int_{-\infty}^{\infty}\int_{-\infty}^{\infty} f(r,s)e^{-i[X(r\cos\theta - s\sin\theta)+Y(r\sin\theta+s\cos\theta)]}drds$$
$$= F_\theta(R,S) ,$$

where R and S are $X\cos\theta+Y\sin\theta$ and $Y\cos\theta-X\sin\theta$ respectively. From the rotated function $f_\theta(r,s)$, the projection is

$$p_\theta(r) = \int_{-\infty}^{\infty} f_\theta(r,s)ds ,$$

and the Fourier transform of $p_\theta(r)$ being

$$P_\theta(R) = \int_{-\infty}^{\infty}\int_{-\infty}^{\infty} f_\theta(r,s)e^{-iRr}dsdr .$$

Comparing $P_\theta(R)$ with $F_\theta(R,S)$ it appears that $P_\theta(R)$ is equivalent to $F_\theta(R,S)$ along R or

$$P_\theta(R) = F_\theta(R,S)\big|_{S=0} .$$

The above equation is the "Projection-Slice theorem" which states that the one-dimensional Fourier transform of a projection is a "slice" through the two-dimensional Fourier transform of the original function.

3.2 The Reconstruction Formula

It follows from the Projection-Slice theorem that if an infinite number of Fourier slices are taken from the corresponding infinite number of projections, $F(X,Y)$ would be known at all points in the (X,Y) plane.

Knowing $F(X,Y)$, the function $f(x,y)$ can be recovered by using the inverse Fourier transform:

$$f(x,y) = \frac{1}{4\pi^2}\int_{-\infty}^{\infty}\int_{-\infty}^{\infty} F(X,Y)e^{i(Xx+Yy)}dXdY .$$

Rewriting the above equation in polar coordinates we have

$$f(x,y) = \frac{1}{4\pi^2}\int_0^{2\pi}\int_{-\infty}^{\infty} F(R,\theta)e^{iR(x\cos\theta+y\sin\theta)}RdRd\theta .$$

The function $F(R,\theta)$ is equivalent to $F_\theta(R,S)\big|_{S=0}$ or to $P_\theta(R)$ by the Projection Slice theorem. Also $F_{\theta+180}(-R,S)$ is $F_\theta(R,S)$, hence,

$$f(x,y) = \frac{1}{4\pi^2}\int_0^{\pi}\int_{-\infty}^{\infty} P_\theta(R)e^{iRr}|R|dRd\theta .$$

The above integral is not bounded since $|R|$ dose not converge. Therefore R should be limited to some value $|R| \le \Omega$. We now introduce a band limited filter $H(R) = b(R)|R|$ where

$$b(R) = \begin{cases} 1 & if\ |R| \le \Omega \\ 0 & if\ |R| > \Omega \end{cases} .$$

The lateral sampling has an interval "a", hence by the sampling theorem,

$$\Omega = 2\pi f_{max} = \frac{\pi}{a} .$$

Replace $|R|$ by $H(R)$ and use the convolution theorem to give the required reconstruction formula

$$f(x,y) = \frac{1}{2\pi}\int_0^{\pi}\int_{-\infty}^{\infty} p_\theta(\tau)h(x\cos\theta + y\sin\theta - \tau)d\tau d\theta ,$$

where $h(r)$ is the inverse Fourier transform of $H(R)$ which can be written analytically as

$$h(r) = \begin{cases} \frac{\Omega^2}{2\pi} & ,r = 0 \\ \frac{1}{2\pi}\left[\frac{2\Omega}{r}\sin(\Omega r) + \frac{2}{r^2}\cos(\Omega r) - \frac{2}{r^2}\right] & ,r \ne 0 \end{cases} .$$

3.3 Numerical Implementation

The filter function $h(r)$ is written into a discrete from $h(r_k=ak)$ for $k = 0,1,...,M-1$ as

$$h(0) = \frac{\pi}{2a^2}$$
$$h(r_k) = -\frac{2}{\pi k^2 a^2} \quad ,k = odd$$
$$h(r_k) = 0 \quad ,k = even .$$

The above equations define the "Ramachandran filter function" (RMCD)(see Fig.5) which is found to be somewhat oscillatory. Shepp and Logan [7], introduce another filter with a more damped response,

$$h(r_k) = -\frac{4}{\pi a^2(4k^2 - 1)} \quad ,k = 0,\pm1,...,\pm(M-1) .$$

This equation is called the "Shepp and Logan filter function" (SL)(see Fig.6).

Therefore, the discrete approximation for the filter back-projection formula can be written as

$$f(x,y) = \frac{a}{2N}\sum_{j=1}^{N}\sum_{k=1}^{M} p_{\theta_j}(r_k)h(x\cos(\theta_j) + y\sin(\theta_j) - r_k) ,$$

where M is the number of sampling points and N the number of sampling angles.

4. Reconstruction Results and Discussions

Effects of sampling rate and measurement noise on reconstruction accuracy are studied in this section by using FBP technique to reconstruct two simple profiles: Gaussian and multi-

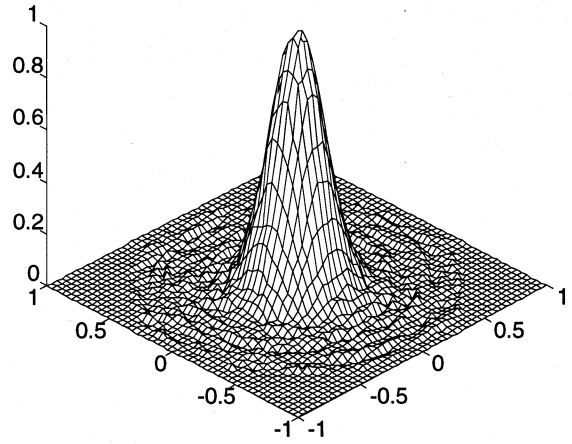

(a)

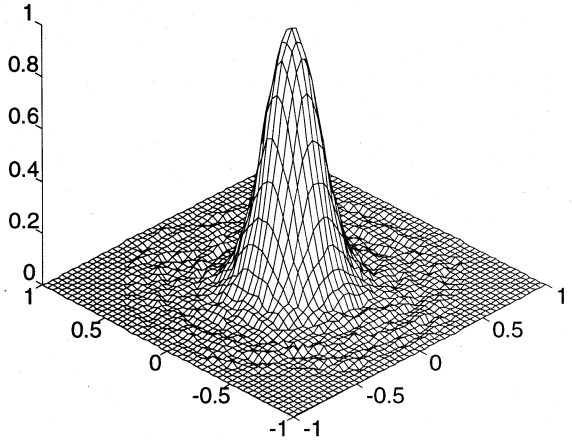

(b)

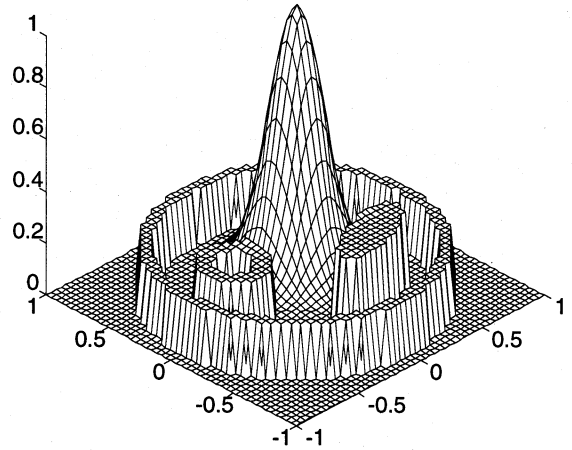

(c)

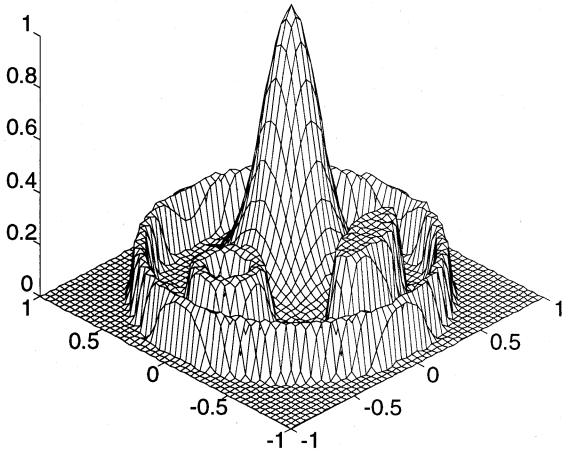

(d)

Figure 12 Reconstruction result of :-

(a) Gaussian profile with RMCD filter with noise added (M=64, N=90)

(b) Gaussian profile with SL filter with noise added (M=64, N=90)

(c) True function of off-center Gaussian profile with obstacles

(d) Off-center Gaussian profile with obstacles (M=64, N=90) without noise (use SL filter function)

layer top hat. Each test profile has different characteristics both in space and frequency domains. We also advance the technique to reconstruct a combination of Gaussian and ellipsoid functions from their projections in order to demonstrate its capability for reconstructing an arbitrary two dimensional function.

It is shown in Fig. 7 and Fig. 8 that small angular sampling rates has a considerable effect on the reconstruction results. This is because the filter function used in this study contains a large difference between its highest positive value and lowest negative value (Fig 5a), yielding deep negative values and high positive values of the back project filtered function in the space domain. These values from such view angles cannot be compensated by the summation of a few sampling angles and hence noise-like patterns appear. It is shown in the picture distance measurement (Fig. 9), especially in the multi-layer top hat profile, that whenever we try to catch the high frequency signal by increasing the lateral sampling rate (in order to meet the sampling theorem requirement and to reduce Gibbs phenomenon [4]), we are forced to increase the angular sampling rate, otherwise the noise-like patterns will appear. Choosing filter functions that exhibit a small difference between the highest positive value and the lowest negative value (for example, see SL filter Fig. 6a) is another way to reduce this noise-like pattern. Then less angular samplings are needed to compensate the over and under-shooting effect of the filter function used (compare Fig. 12a with b).

The effect of measurement noise on reconstruction results can be evaluated by comparing the reconstruction from noisy projections (fictitious noise in our case) with the one from noise free projection. Fig. 10 shows the projection of the Gaussian function, corrupted with fictitious random noise of magnitude limited to 1% of the maximum value of the projection data. Since the Fourier transform of a Gaussian is also a Gaussian then the Fourier components should have decayed exponentially with increasing frequency. Conversely, in this particular case, the corrupted noise appears as the high frequency Fourier components and hence increasing the lateral sampling rate means introducing more noisy components into the reconstruction process. This results in a larger value of the picture distance as shown in Fig 11. Using the SL filter improves the reconstruction results (see both Fig.11 and Fig.12). This is because the SL filter is less sensitive to the high frequency signal than the RMCD, as already shown in Fig. 6. Therefore in the case of reconstruction from noisy projections, the SL filter is preferred.

The above discussions are applicable for the reconstruction of an asymmetric profile. Fig. 12 shows an arbitrary two dimensional test function and its FBP reconstruction result. The Gibbs errors due to discontinuity can be reduced by increasing the lateral sampling frequency. This, however, should be accompanied with the increasing angular sampling so that the noise-like pattern is minimized. Since measurement noise is not involved then RMCD filter is preferred.

5. Conclusion and Future Directions for Research

The FBP algorithm for reconstructing mean combustion field property from their computer simulated data has been evaluated. The major practical limitation of the method appears to be the need for many angular viewing angles. This is partly due to the choice of inversion method: mathematical transforms methods are not best suited to Gaussian profiles. Improved algorithms and filters should be evolved.

Also recent techniques have been used outside of the combustion diagnostics field: pattern recognition and maximum entropy methods come to mind. Current research on wavelets seem to be relevant to this particular problem. For practical purpose, a method tolerant of limited angular access (industrial combustors) would be most desirable. A more advanced tomographic algorithms for reconstructing fluctuating fields such as fluctuating property field in turbulent flames is also a challenging research area.

References

[1] Hughey, B. J. and Santavicca, D.A., 1982, "A Comparison of Techniques for Reconstructing Axisymmetric Reacting Flow Fields from Absorption Measurements", *Combustion Science and Technology*, Vol.29, pp.167-190.

[2] Chen, F.P. and Goulard, R. ,1976, "Retrieval of Arbitrary Concentration and Temperature Fields by Multiangular Scanning Techniques." *J.Q.S.R.T 16*, pp. 819-827.

[3] Emmerman, P.J.,Goulard, R.,Santoro, R.J.,and Semerjian, H.G. ,1980, *AIAA J.4* No.2:70.

[4] Bracewell, R.N., 1986, *The Fourier Transform and its Applications*, McGraw-Hill, Inc., New York.

[5] Shigehito Suzuki, 1983, "A study on the resemblance between a computed tomographic image and the original object, and the relationship to the filter function used in image reconstruction", *Optik 66*, No.1, pp. 61-71.

[6] Azriel Rosenfeld, Avinash C. Kak, 1982, *Digital Picture Processing*, 2nd Edition, Vol. 1, Academic press.

[7] Shepp, L. A. and Logan, B. F. , 1974, "The Fourier Reconstruction of a Head Section", *IEEE Transactions on Nuclear Science*, Vol. NS-21, pp. 21-40.

Acknowledgment

This work was supported in part by The Thailand Research Fund , Grant No. PDF/53/2540.

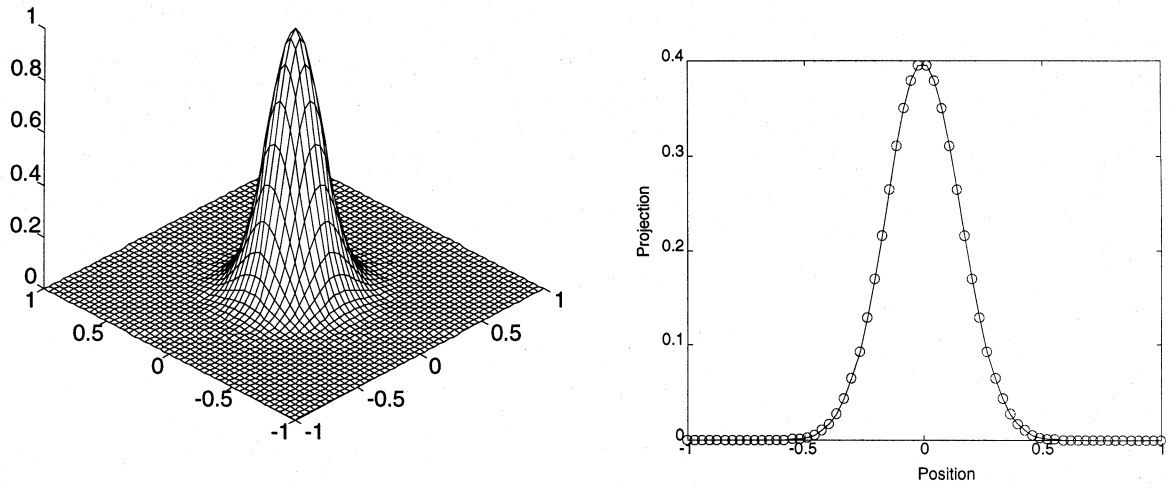

Figure 3 True function of Gaussian profile and its projection.

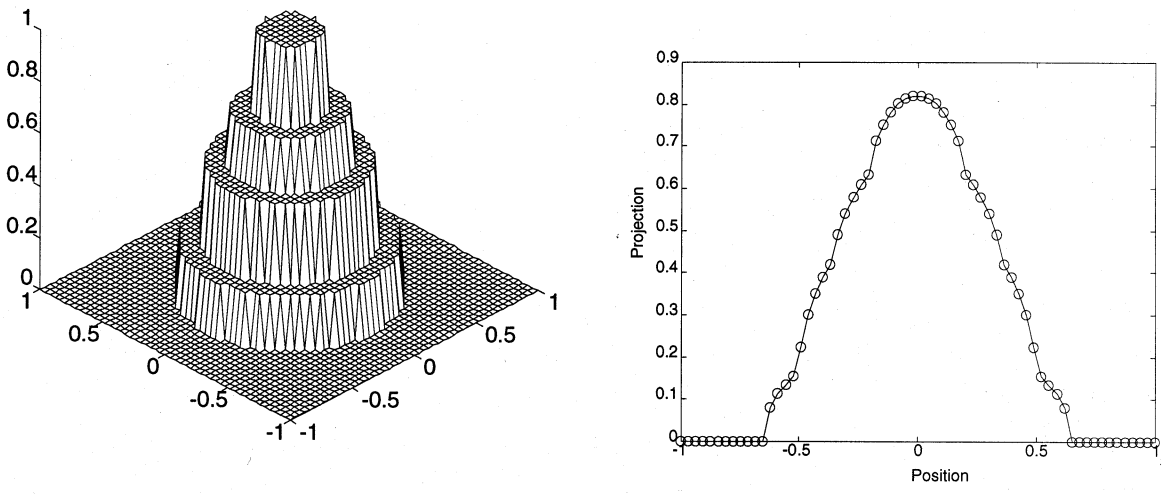

Figure 4 True function of multi-layer top hat profile and its projection.

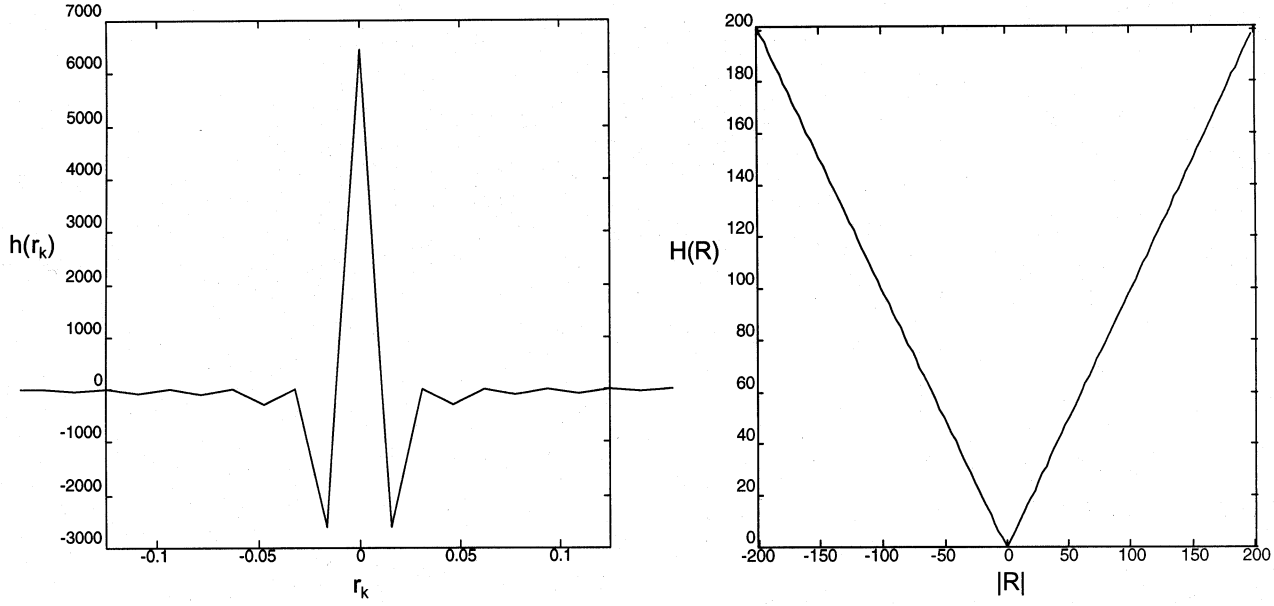

Figure 5 Ramachandran filter function in spatial domain (a) and frequency domain (b) with M=128

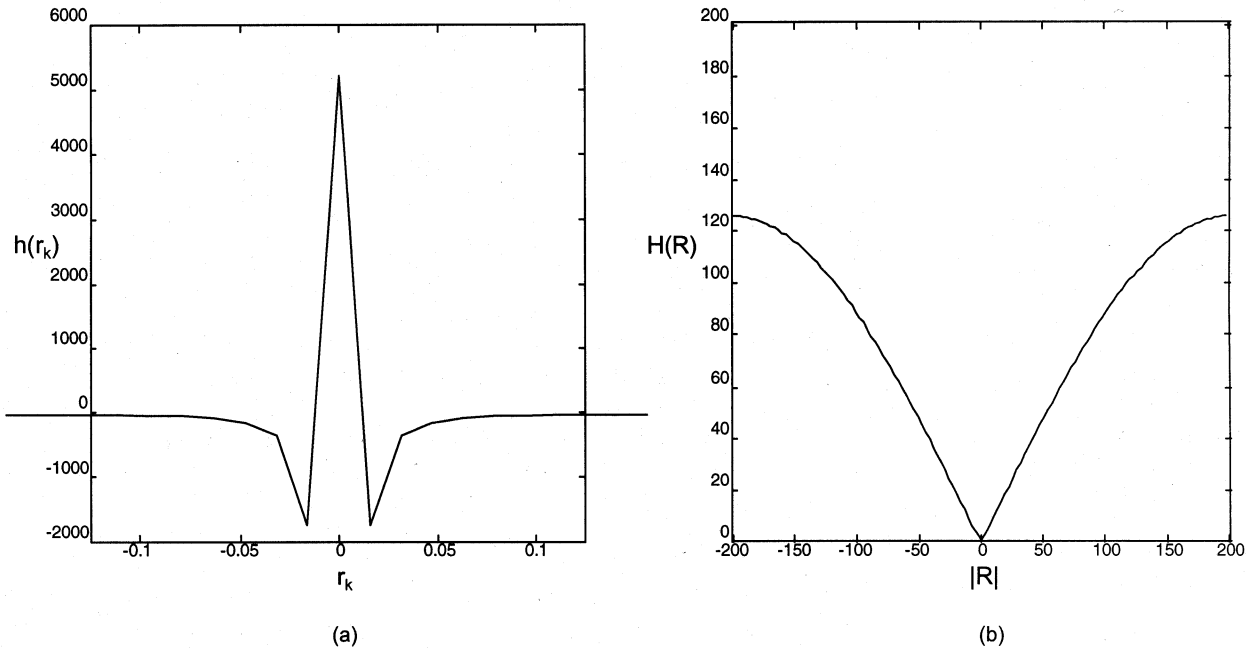

Figure 6 Shepp and Logan filter function in spatial domain (a) and frequency domain (b) with M=128

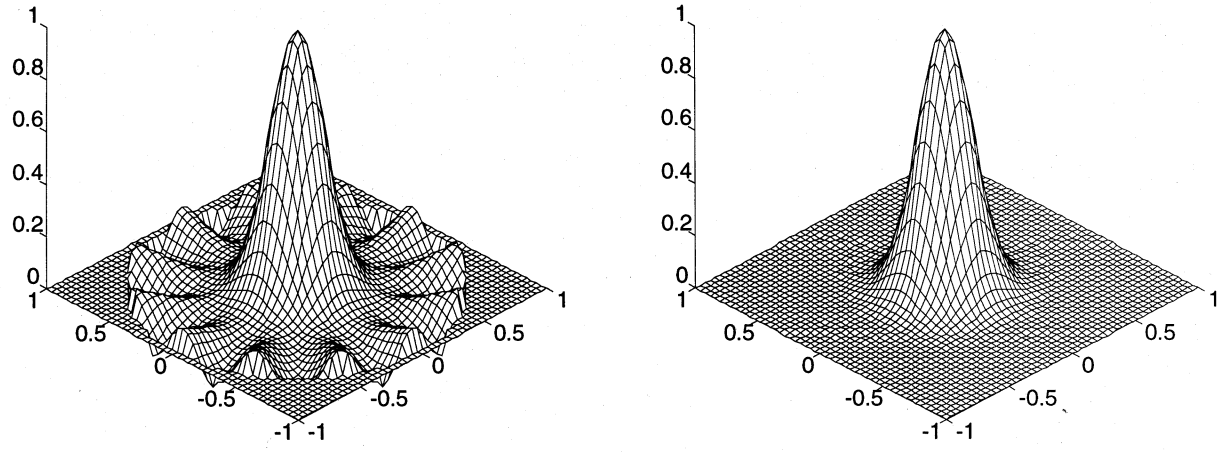

Figure 7 Reconstruction result of Gaussian profile with 64 sampling points
(a) 6 sampling angles and (b)18 sampling angles

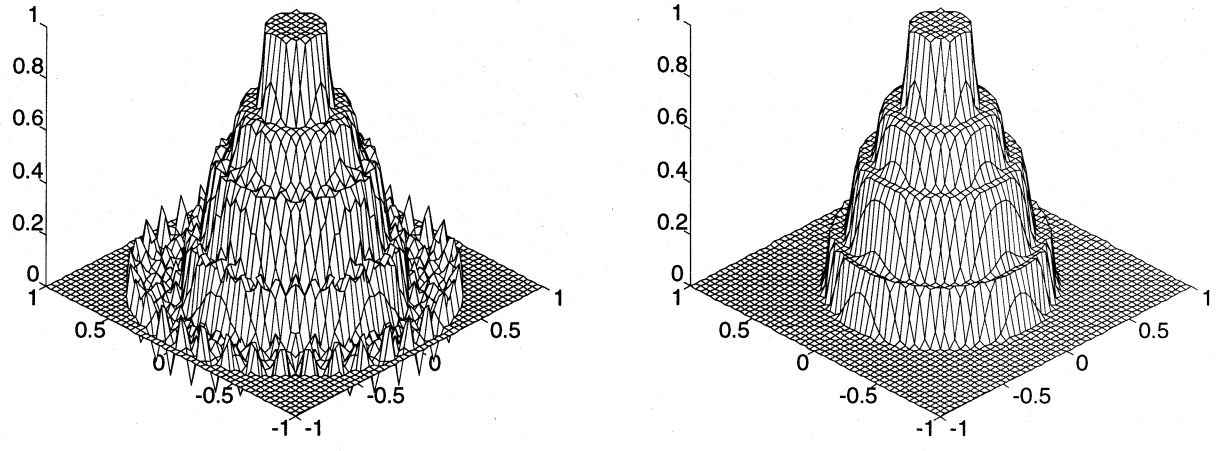

Figure 8 Reconstruction result of multi-layer top hat profile with 64 sampling points
(a) 18 sampling angles and (b) 180 sampling angles

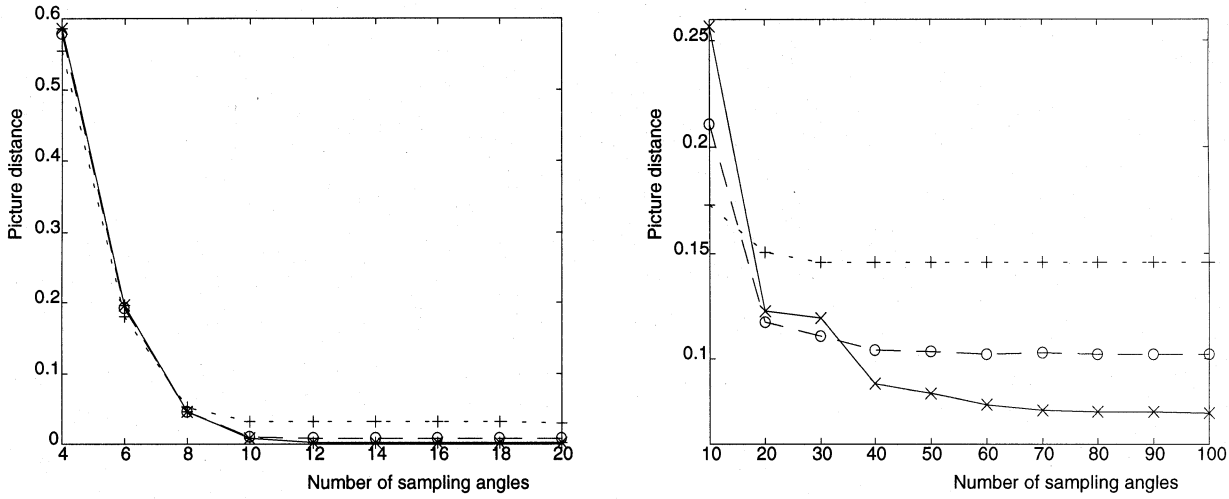

Figure 9 Picture distance as a function of the number of sampling angles of (a) Gaussian profile, (b) multi-layer top hat profile

32 sampling points

64 sampling points

128 sampling points

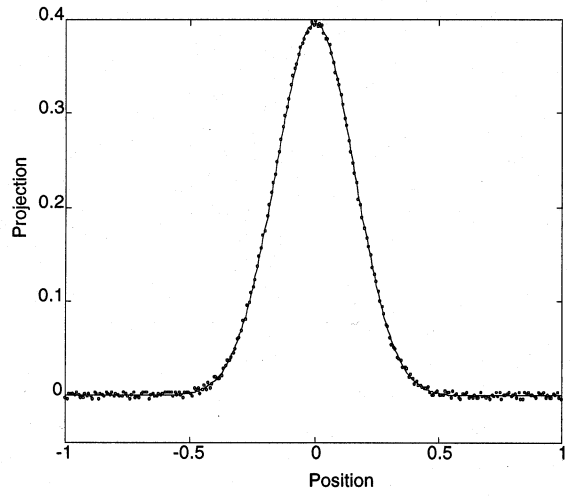

Figure 10 Projection of Gaussian profile with 1% maximum random noise added

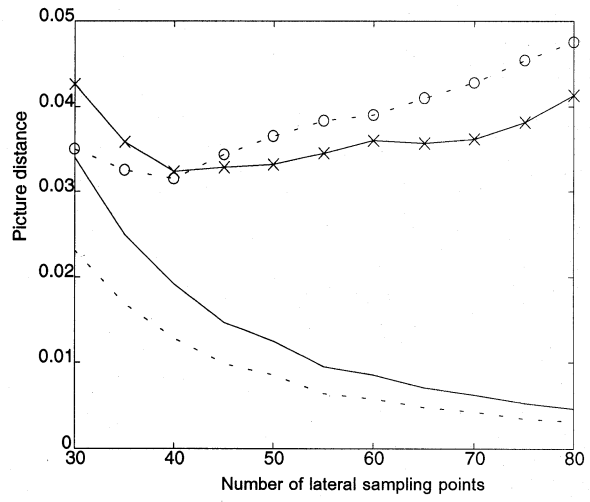

Figure 11 The effect of noise and the comparison of efficiency of filter functions at constant number of sampling angles (90 angles)

Ramachandran filter function with noise added

Shepp and Logan filter function with noise added

Ramachandran filter function without noise

Shepp and Logan filter function without noise